Biosensors and Bioelectronics 145 (2019) 111704

Contents lists available at ScienceDirect

Biosensors and Bioelectronics

journal homepage: www.elsevier.com/locate/bios

CuO nanoparticles derived from metal-organic gel with excellent electrocatalytic and peroxidase-mimicking activities for glucose and cholesterol detection

Qing Wu[a], Li He[a], Zhong Wei Jiang[a], Yang Li[a], Zheng Mao Cao[a], Cheng Zhi Huang[b,**], Yuan Fang Li[a,*]

[a] Key Laboratory of Luminescent and Real-Time Analytical Chemistry (Southwest University), Ministry of Education, College of Chemistry and Chemical Engineering, Southwest University, Chongqing, 400715, China
[b] College of Pharmaceutical Science, Southwest University, Chongqing, 400715, China

ARTICLE INFO

Keywords:
CuO nanoparticles
Metal–organic gel
Electrocatalytic
Peroxidase-mimicking

ABSTRACT

A simple and efficient strategy was developed to fabricate CuO nanoparticles (CuO-NPs) with high surface area by the direct pyrolysis of a metal-organic gel (MOG) precursor for constructing versatile catalytic interfaces. Unexpectedly, the obtained CuO-NPs exhibited excellent electrocatalytic activity for glucose (Glu) oxidation reaction. The linear range of glucose was from 5 μM to 600 with the detection limit of 0.59 μM. Additionally, the CuO-NPs showed distinguished intrinsic peroxidase-mimicking activities, which can be further used as biomimetic nanozymes for sensitively and rapidly detecting cholesterol. A good linearity of cholesterol was performed in the range from 1 μM to 15 μM with the detection limit of 0.43 μM. The as-prepared CuO-NPs could provide a versatile catalytic platform for the application of electrochemical sensors and biomimetic enzyme catalytic systems. This study proved the high potential of MOG-derived nanostructured transition metal oxides (TMOs) with multiple complex functions.

1. Introduction

Substantial research efforts are directed toward the utilization of nanomaterials in catalytic systems(Brahman et al., 2016; Chen et al., 2018a; Hu et al., 2017b; Huang et al., 2017; Muench et al., 2017; Reddy et al., 2018; Song et al., 2019; Suresh et al., 2018; Zheng et al., 2018). However, to the best of our knowledge, nanomaterials with collective catalytic properties such as high electrocatalytic activity and enzyme-mimicking activities have rarely been reported. Among these available nanocatalysts, transition metal oxides (TMOs) have received much attention in the field of catalysis owing to their higher exposed metal active sites(Chen, et al., 2018b; Ling et al., 2018; Natalio et al., 2012; Tanaka et al., 2018; Xu et al., 2019). Copper oxide (CuO), an important member of the TMOs family, is considered as a promising catalytic material owing to its abundant active sites, chemical stability, low-cost and environmental benignity(Ko et al., 2012; Poizot et al., 2000; Wang et al., 2011). To date, different CuO nanomaterials fabricated by various methods including microwave synthesis (Foroughi et al., 2017; Zheng et al., 2016), thermal oxidation (Guo et al., 2012; Huang et al., 2014), templated synthesis (Yang et al., 2016), chemical etching (Huang et al., 2015) have been reported to be used as electrocatalysts or nanozymes. However, the unsatisfactory catalytic activities or the complex synthesis of CuO nanomaterials limits their further applications in different fields. Clearly, it is still highly desirable to develop a simple, efficient and cost-effective strategy for fabricating porous CuO nanomaterials with the versatile catalytic properties of high electrocatalytic activity and enzyme mimicking.

Metal-organic gel (MOG) is an emerging smart soft material that is rapidly straightforwardly self-assembled from metal ions and organic ligands through metal-ligand interactions and intermolecular forces(He et al., 2018; Tam and Yam, 2013; Wu et al., 2019a). MOG have been an increasing interest in the fields of separation (Jayaramulu et al., 2017; Karan and Bhattacharjee, 2016), sensing (Li et al., 2018; Lin et al., 2016), catalysis (He et al., 2017, 2018), drug delivery (Li et al., 2010; Tan et al., 2016) and light-emitting diodes (Kamtekar et al., 2010; Sun et al., 2006) due to their intrinsic and desirable characteristics of porosity, large surface area, low molecular weight and high thermal stability(Wang et al., 2017). More interestingly, other than their direct

* Corresponding author.
** Corresponding author.
E-mail addresses: chengzhi@swu.edu.cn (C.Z. Huang), liyf@swu.edu.cn (Y.F. Li).

https://doi.org/10.1016/j.bios.2019.111704
Received 25 June 2019; Received in revised form 22 August 2019; Accepted 13 September 2019
Available online 14 September 2019
0956-5663/

use, MOG have been recently employed as a novel attractive precursor for the preparation of different nanomaterials. For instance, Fe_xO_y/nitrogen-doped carbon films derived from Fe-based MOG for enhanced lithium storage(Yang et al., 2018). The carbonization of Cr-based MOG in an inert atmosphere to produce nitrogen-doped porous carbon material could be used for small biomolecular sensing(Shih et al., 2017). Magnetic porous carbon was efficiently remove organic dyes by using Fe-based MOG as a template(Wang et al., 2016). Nevertheless, despite the above progress and achievements, nanostructured TMOs with high surface area derived from MOG has rarely been reported. Therefore, it is highly possible to prepare CuO nanostructures by using MOG as a precursor due to its facile synthesis and the desirable characteristics of large specific surface areas, porosities, stability and ultrahigh metallic dispersion.

Herein, a simple and efficient strategy was developed to synthesize CuO nanoparticles (CuO-NPs) with high surface area as a versatile catalytic nanomaterial by thermal decomposition of Cu-based metal-organic gel (Cu-MOG) precursor. As shown in Scheme 1, the CuO-NPs showed high electrocatalytic activity for glucose (Glu) oxidation and distinguished peroxidase-like catalytic activities. The versatile catalytic functions of CuO-NPs could provide a promising platform for developing a bioanalysis and sensing system. Moreover, the strategy for the utilization of MOG as a novel and potential precursor to prepare CuO nanostructures with high surface area provided new promising applications of the rapidly growing MOG family.

2. Experimental

2.1. Synthesis of CuO-NPs

Firstly, Cu-MOG was synthesized rapidly by a one-step mixing method. Briefly, 0.02 M $CuSO_4{\cdot}5H_2O$ and 1,3,5-tris(4,-carboxyphenyl) (H_3BTB) were mixed in an equal volume. Then blue gel was appeared quickly. The as-obtained Cu-MOG was further freeze-dried to completely remove solvents. Subsequently, the dried Cu-MOG was heated to 500 °C for 1 h with a ramp of 2 °C min^{-1} in air. Finally, the color of the final product changed from blue to black.

2.2. Electrochemical experiments for Glu detection

Firstly, glassy_carbon_electrode (GCE) were polished with 0.05 μm alumina powder and washed in ethanol and H_2O under ultrasound conditions, respectively. Next, 7.0 μL of 1.0 mg mL^{-1} dispersion of CuO-NPs aqueous solution was cast on the GCE (CuO-NPs/GCE) and dried at room temperature. Cyclic voltammetry (CV) was measured in

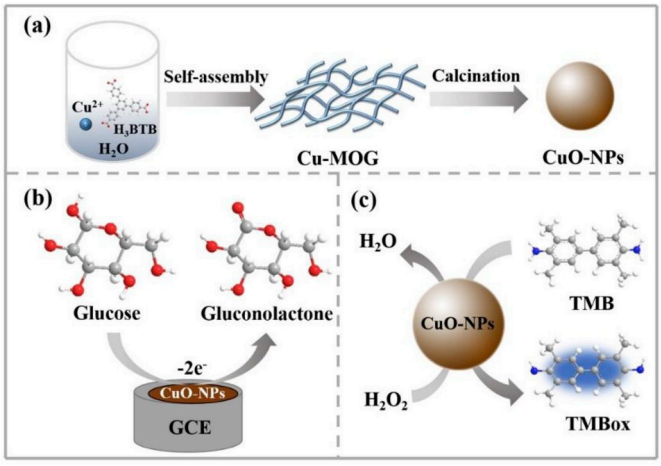

Scheme 1. (a) The fabrication of the CuO-NPs. (b) Electrocatalytic activity and (c) enzyme-mimicking activities of the CuO-NPs.

0.1 M NaOH electrolyte at a scan rate of 50 mV s^{-1}. To study the change of electrocatalytic current with Glu concentration, the current-time response of the CuO-NPs to successively add 100 μM Glu in 0.1 M NaOH was investigated at an operating voltage of 0.55 V. The selectivity for Glu oxidation were also performed under optimal experimental conditions.

2.3. Biomimetic enzyme catalytic activity for detecting cholesterol

Stock solution of cholesterol (1 mM) was prepared in anhydrous ethanol. In a typical method, 50 μL of 1.145 U·mL^{-1} cholesterol oxidase (ChOx) were added to 0.1 mL different concentration of cholesterol diluted with phosphate buffered saline (PBS, 0.5 mM, pH 7.4). Then the mixture solution incubated at 37 °C for 1 h in the dark. Next, 100 μL of Na_2HPO_4 buffer solution (20 mM, pH 4.0), 50 μL of CuO-NPs (1 mg mL^{-1}) solution, 100 μL of TMB (10 mM), and 600 μL deionized water were mixed. Finally, the absorbance spectra was recorded after incubating the mixture solution at 70 °C for 20 min.

2.4. Detection of glu and cholesterol in serum samples

Initially, the human blood acquired from healthy volunteers was first treated by spin dialysis at 10000 rpm for 30 min. For the detection of Glu in human serum, the current-time response of 100 μL of human serum or a mixture of certain amount of Glu (1 mM, 2 mM and 4 mM) in 20 mL of 0.1 M NaOH solution at 0.55V was recorded. While detecting cholesterol in human serum, the serum sample was diluted 50-fold with 0.5 mM PBS solution and adding cholesterol with different concentrations (2 μM, 4 μM and 6 μM), which was incubated with ChOx for 1 h at 37°C. The subsequent procedures are consistent with the mentioned above procedures for cholesterol detection.

3. Results and discussion

3.1. Characterization

Thermogravimetric (TG) analysis (Fig. S1) suggested that Cu-MOG lost weight seriously at about 400 °C and had almost no more weight loss with increasing temperature. From which it can be inferred that the simultaneous formation of stable and pure CuO-NPs at temperatures above 400 °C. Furthermore, scanning electron microscope (SEM) images of Cu-MOG calcined at different temperatures in air indicated that Cu-MOG precursor converted to CuO-NPs at 500 °C (Fig. S2a ~ d). The as-prepared Cu-MOG showed entangled fibrillar nature (Fig. S2a). After the pyrolysis, SEM was used to reveal the morphological changes of the Cu-MOG at different calcination temperatures for 1 h under air condition. In the first temperature gradient of 300 °C, it was found that the pyrolysis of Cu-MOG was not complete from its remaining fibrous structure (Fig. S2b). When the temperature heated to 400 °C, it showed that tiny nanoparticles formed nanofibers by "head-to-head" connection from the SEM image (Fig. S2c). Most of CuO-NPs had an average size of ~45 nm after calcined at 500 °C (Fig. S2d). Additionally, the obtained CuO-NPs product had almost no mass loss from 25 °C to 900 °C, which also indicated that Cu-MOG was completely transformed into CuO (Fig. S1).

X-ray diffraction (XRD) pattern of the final product showed that all reflections in the 2θ range of 20–80°, are consistent with a pure CuO polycrystalline phase (PDF 45–0937) (Fig. 1a). The high crystalline structure of CuO-NPs was inferred from the strong and sharp peaks. In addition, a significant amount of Cu and O species were determined by X-ray photoelectron spectrometry (XPS) (Fig. S3a). The high-resolution Cu 2p spectrum of CuO-NPs signaled with Cu $2p_{3/2}$ and Cu $2p_{1/2}$ peaks at 934 and 954 eV, respectively (Fig. 1b). Moreover, the energy difference was ~20 eV between the peaks of Cu $2p_{3/2}$ and Cu $2p_{1/2}$, in agreement with the characteristics of CuO(Hu et al., 2017a; Martin et al., 2013). Moreover, two strong shake-up peaks were observed at

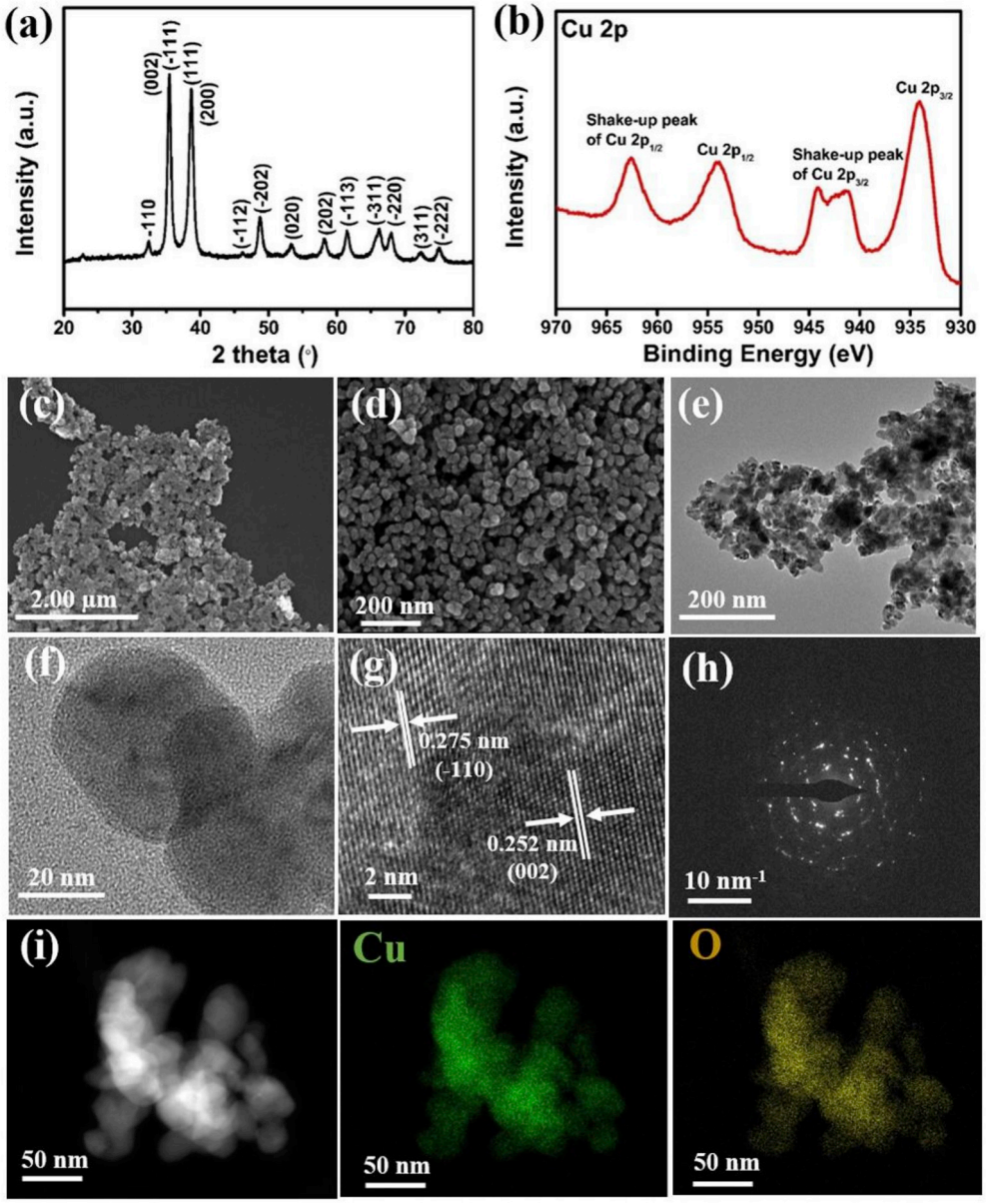

Fig. 1. (a) XRD pattern, (b) high-resolution Cu 2p spectra of CuO-NPs. Morphology and structural characterization of CuO-NPs: (c, d) SEM images, (e, f) TEM images, (g) HRTEM image, (h) SAED pattern and (i) EDS mapping images.

higher binding energies than the main peaks, indicating the presence of unfilled Cu $3d^9$ shell, which was further confirmed the formation of CuO(Liang et al., 2019; Sedighi et al., 2019).

The morphologies of CuO-NPs was characterized by SEM, transmission electron microscope (TEM) and high-resolution TEM (HRTEM). Solid spherical crystals were formed on a large scale, which showed the transformation from nanofibrous Cu-MOG to nano-sized CuO-NPs after the calcination route (Fig. 1c∼f). The d-spacings of the lattice fringes were measured to be 0.275 and 0.252 nm, corresponding well to the (−110) and (002) reflections of CuO from the lattice resolved HRTEM image (Fig. 1g). The corresponding selected area electron diffraction (SAED) pattern (Fig. 1h) showed multiple diffraction rings, which also indicated the polycrystalline structure of CuO-NPs. Energy dispersive spectroscopy (EDS) analysis (Fig. S3b) and elemental mapping analysis (Fig. 1i) further confirmed that only Cu and O species were contained and distributed homogenously across the entire architecture. The presence of Ni was due to the Ni grid support used in the EDS measurement. The surface area and porous structures of CuO-NPs was investigated by nitrogen adsorption–desorption isotherm. It can be classified as typical type IV curves with a hysteresis loop extending within the high relative pressure range of 0.8–1.0, generally ascribed to the mesoporous structure (Fig. S4).(Chen et al., 2012; Wang et al., 2018) The average pore diameter was ∼2.5 nm, which was revealed by the Barrett-Joyner-Halenda (BJH) method (inset). Furthermore, the CuO-NPs exhibited a high Brunauer-Emmett-Teller (BET) surface area of 20.16 $m^2 g^{-1}$ and a high pore volume of 0.11 $cm^3 g^{-1}$, which was much higher than the reported CuO nanostructures (Hu et al., 2013; Xiao et al., 2016; Yuan et al., 2012; Zeng et al., 2018; Zhang et al., 2015).

3.2. Electrochemical performance

The electrocatalytic behavior of CuO-NPs towards Glu oxidation was evaluated. As the concentration of Glu increased, the anodic currents were gradually enhanced (Fig. 2a), corresponding to irreversible Glu oxidation, which demonstrated the significant electrocatalytic activity of CuO-NPs to Glu. Glu oxidation appeared in the range of 0.30–0.70 V, which was ascribed to the conversion of Cu (II) to Cu (III)

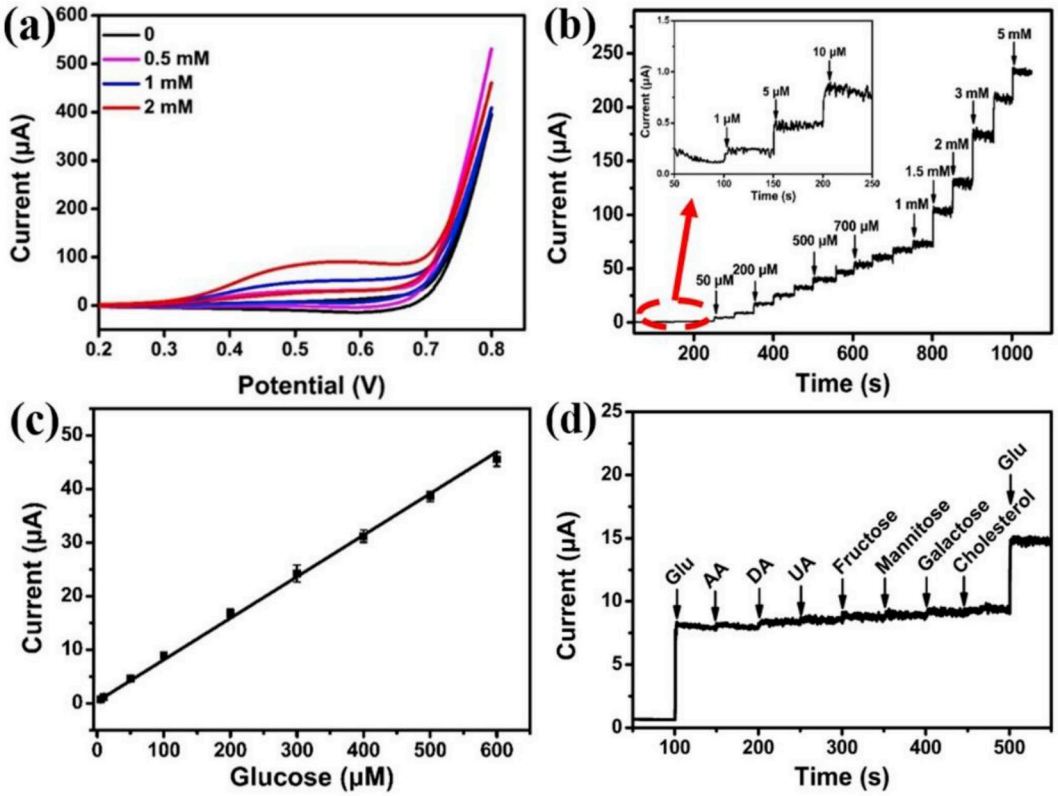

Fig. 2. (a) CV of the CuO-NPs/GCE with different concentrations of Glu. (b) Current–time response of the CuO-NPs/GCE to continuous additions of various amounts of Glu. (c) Electrocatalytic current vs. different concentration of Glu. (d) Amperometric response of CuO-NPs/GCE with addition of 100 μM of Glu, 5 μM of the following interfering species (AA, DA, UA, fructose, mannitose, galactose and cholesterol), and 100 μM Glu.

(Ling et al., 2018; Wu et al., 2010). The CuO/CuOOH redox couple is formed by the oxidation of CuO to CuOOH, which can catalyze the oxidation of Glu(Dong et al., 2015; Ling et al., 2018). The catalytic process was as follows for Glu oxidation.

$$CuO + OH^- \rightarrow CuOOH + e^- \quad (1)$$

$$CuOOH + e^- + \text{glucose} \rightarrow CuO + OH^- + \text{gluconolactone} \quad (2)$$

The electrochemical performances of the different electrodes were also compared by CV in the absence and presence of Glu (Fig. S5a). It was obvious that one stable and strong oxidation peak occurred in the presence of Glu for CuO-NPs/GCE, which demonstrated that the catalytic oxidation of Glu mainly resulted from the active site of CuO. Furthermore, the conductive properties of CuO-NPs was evaluated by the electrochemical impedance spectroscopy (EIS) (Fig. S5b). It was obvious that the charge transfer resistance (Rct) of CuO-NPs/GCE was lower than that of GCE and MOG, implying the good conductive properties of CuO-NPs.

Prior to nonenzymatic Glu sensing, the optimum working potential was investigated by the successive addition of Glu at various potentials from 0.45 V to 0.65 V (Fig. S6a), which indicated that 0.55 V was suitable for detecting Glu. As observed, the current-time response of the CuO-NPs to successively add Glu (Fig. 2b). Moreover, the electrocatalytic current was good linear to the Glu concentration from 5 μM to 600 μM with the equation I (μA) = 0.3633 + 0.0776C (μM), R^2 = 0.9983. The detection limit was 0.59 μm at S/N = 3 (Fig. 2c) with a sensitivity of 1098.37 μA mM^{-1} cm^{-2}. The new electrochemical sensor had significant sensitivity and lower detection limits compared with most previously reported sensors for nonenzymatic detection of Glu (Table 1).

Amperometric selectivity for detecting Glu was evaluated by the addition of other interfering species including ascorbic acid (AA), dopamine (DA), uric acid (UA) and fructose, mannitose, galactose and cholesterol. The current responses of Glu showed notable increase, whereas these interfering species produced a minimal current response (Fig. 2d). The observations suggested the excellent sensitivity and selectivity of CuO-NPs to electrocatalytic oxidation of Glu. A good stability of the as-prepared CuO-NPs for Glu detection was demonstrated (Fig. S6b). Additionally, to confirm its feasibility for practical applications, we investigated the spiked recoveries of Glu by adding a certain amount of standard solution of Glu to the serum samples. Table S1 showed the corresponding recovery values recovery of 96–107%, demonstrating that the method was suitable for detecting Glu in human serum samples.

3.3. Peroxidase-mimetic activity of CuO-NPs

Development of biomimetic enzymes mimicking the native enzyme attracts growing interest(Lin et al., 2018; Liu et al., 2012; Wu et al., 2019b; Yao et al., 2018). To test the catalytic activity CuO-NPs as enzyme mimics, we researched the enzyme-mimicking catalytic activity of CuO-NPs in the TMB-H_2O_2 system. The as-synthesized CuO-NPs displayed obvious absorbance for the oxidation of TMB in the presence H_2O_2, while other control groups showed a weak absorbance peak (Fig. S7). This result demonstrated that CuO-NPs displayed excellent peroxidase-mimetic catalytic activity. Therefore, we suggest that the CuO-NPs–TMB–H_2O_2 system could be applied as colorimetric assay platform for analyzing the substrates of H_2O_2-generating oxidases, such as cholesterol. Prior to analyze cholesterol, the experimental conditions, including reaction time, pH, temperature, CuO-NPs concetrations and the dose of ChOx (1.145 U·mL^{-1}) were optimized (Fig. S8a ~ e). Under the optimal assay conditions, the standard curve for cholesterol was constructed within the concentration range from within the wide range of 1 μM–15 μM with the detection limit of 0.43 μM (S/N = 3) (ΔI = 0.00706C + 0.01218, R^2 = 0.994; ΔI is the change of absorbance

Table 1
Comparison of different electrochemical sensors for glucose.

Electrode material	Linear range (μM)	Detection limit (μM)	Sensitivity (μA ·mM^{-1} cm^{-2})	Reference
Cu_xO/PPy/Au	20–8000	6.2	232.22	Meng et al. (2013)
Co_3O_4 UHMSA	0.1–5	1.84	102.77	Ding et al. (2016)
NiO/Fe_2O_3	1–450	1.03	1437	Jana et al. (2018)
NiO/Fe_2O_3	1–10	1.29	378	Fu et al. (2016)
Ni/Co phosphate	2–4470	0.4	302.99	Shu et al. (2018)
GF/AuNS	–	1.15	1045.9	Peng et al. (2018)
GPL-FePc-CH	1000–20000	6.	18.11	Han et al. (2019)
CuO-NPs	5–600	0.59	1098.37	This work

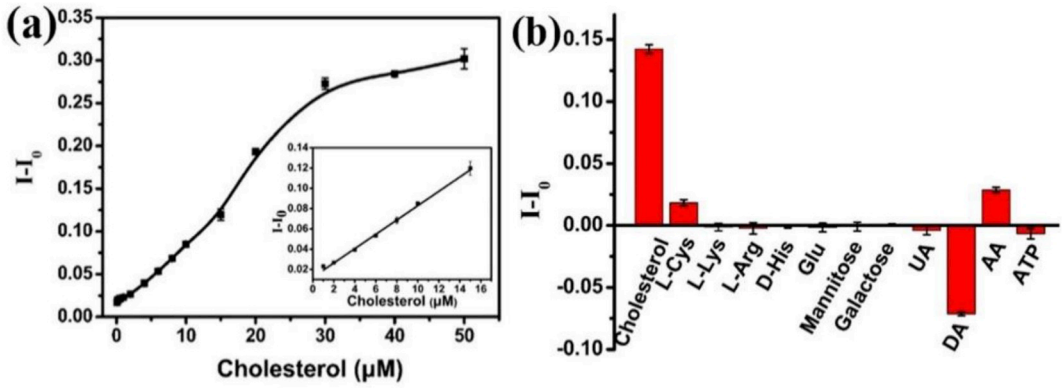

Fig. 3. (a) The linear standard curve for cholesterol determination. (b) Selectivity for detecting cholesterol. The concentration of cholesterol and interfering substances were 15 μM.

Table 2
Comparison of assay performance of different methods for cholesterol.

Materials	Detection method	Linear range (μM)	Detection limit (μM)	Reference
MnO_2	Fluorescence	1–300	0.33	Han et al. (2019)
RGO/AuNP/luminol	CL	0.71–11.43	0.55	Lin et al. (2017)
CSPPy-g-$C_3N_4H^+$	Amperometric	20–5000	8	Shrestha et al. (2017)
ChOx/PtNPs/PANI/MEA	Amperometric	1000–12000	440	Gao et al. (2019)
G/Ti(G)-3DNS/CS/ChO_x	PEC	50–8000	6	Komathi et al. (2016)
MoS_2-GSSG NSs	Colorimetric	5.36–800	5.36	Yin et al. (2018)
BNNS@CuS	Colorimetric	10–100	2.9	Zhang et al. (2017)
CuO-NPs	Colorimetric	1–15	0.43	This work

CL: Chemiluminescence.
PEC: Photoelectrochemical.

value and *C* is the cholesterol concentration, μM) (Fig. 3a). The proposed cholesterol sensor based on the CuO-NPs compared favorably to the behaviors of most reported assays (Table 2).

The selective detection of cholesterol was investigated. As expected, these interferences exhibited negligible responses compared to cholesterol except DA (Fig. 3b), which demonstrated that high selectivity of the CuO-NPs based colorimetric system. The obvious minus effect of DA was probably caused by the spontaneous oxidation of DA by dissolved oxygen in water(Bisaglia et al., 2007; He et al., 2017; Zhuang et al., 2019). As shown in Figs. S8f and a good stability of the CuO-NPs for cholesterol was also displayed. Furthermore, the routine analysis was also performed to verify the reliability of this method by investigating the spiked recoveries of cholesterol in human serum. Different concentrations of standard solution of cholesterol were mixed with the diluted serum samples, respectively. The acceptable recovery rates of 92–109% were obtained (Table S2), which demonstrated that the method was applicable to detect cholesterol in serum samples.

4. Conclusion

In summary, we successfully reported a facile and efficient strategy to prepare CuO-NPs as versatile catalysts by thermal calcination MOG precursor. The as-synthesized CuO-NPs with high specific surface areas, porosities and abundant exposed metal active sites could be successfully used as electrocatalysts and biomimetic nanozymes, which showed high sensitivity and selectivity for the detection of Glu and cholesterol. Consideration the limitations of *in vitro* testing, the further interesting path to examine the cytotoxicity of the CuO-NPs and develop CuO-NPs capable of monitoring intracellular biomolecules is also worthwhile exploration. Furthermore, it is believed that the strategy of MOG derived CuO-NPs would show high potential for the development of more advanced functional nanostructured TMOs in biocatalysis, bioassays, and nano-biomedicines.

CRediT authorship contribution statement

Qing Wu: Conceptualization, Methodology, Investigation, Data curation, Validation, Formal analysis, Writing - original draft. **Li He:** Writing - review & editing. **Zhong Wei Jiang:** Visualization. **Yang Li:** Software. **Zheng Mao Cao:** Software. **Cheng Zhi Huang:** Formal analysis, Writing - review & editing. **Yuan Fang Li:** Funding acquisition, Formal analysis, Writing - review & editing, Project administration.

Declaration of competing interest

The authors declare that they have no known competing financial interests or personal relationships that could have appeared to influence the work reported in this paper.

Acknowledgments

The authors are grateful to the National Natural Science Foundation of China (NSFC, no. 21575117).

Appendix A. Supplementary data

Supplementary data to this article can be found online at https://doi.org/10.1016/j.bios.2019.111704.

References

Bisaglia, M., Mammi, S., Bubacco, L., 2007. Kinetic and structural analysis of the early oxidation products of dopamine: analysis of the interactions with alpha-synuclein. J. Biol. Chem. 282 (21), 15597–15605.

Brahman, P.K., Suresh, L., Lokesh, V., Nizamuddin, S., 2016. Fabrication of highly sensitive and selective nanocomposite film based on CuNPs/fullerene-C_{60}/MWCNTs: an electrochemical nanosensor for trace recognition of paracetamol. Anal. Chim. Acta 917, 107–116.

Chen, L.F., Zhang, X.D., Liang, H.W., Kong, M., Guan, Q.F., 2012. Synthesis of nitrogen-doped porous carbon nanofibers as an efficient electrode material for supercapacitors. ACS Nano 6 (8), 7092–7102.

Chen, W.H., Vazquez-Gonzalez, M., Kozell, A., Cecconello, A., Willner, I., 2018a. Cu(2+)-modified metal-organic framework nanoparticles: a peroxidase-mimicking nanoenzyme. Small 14 (5), 1703149.

Chen, X.M., Shi, Z.X., Hu, Y.F., Xiao, X.H., Li, G.K., 2018b. A novel electrochemical sensor based on Fe3O4-doped nanoporous carbon for simultaneous determination of diethylstilbestrol and 17β-estradiol in toner. Talanta 188, 81–90.

Ding, L.J., Zhao, M.G., Fan, S.S., Ma, Y., Liang, J.J., Wang, X.T., Song, Y.W., Chen, S.G., 2016. Preparing Co_3O_4 urchin-like hollow microspheres self-supporting architecture for improved glucose biosensing performance. Sens. Actuators, B 235, 162–169.

Dong, C., Zhong, H., Kou, T., Frenzel, J., Eggeler, G., Zhang, Z., 2015. Three-dimensional Cu foam-supported single crystalline mesoporous Cu_2O nanothorn arrays for ultrahighly sensitive and efficient nonenzymatic detection of glucose. ACS Appl. Mater. Interfaces 7 (36), 20215–20223.

Foroughi, F., Rahsepar, M., Hadianfard, M.J., Kim, H., 2017. Microwave-assisted synthesis of graphene modified CuO nanoparticles for voltammetric enzyme-free sensing of glucose at biological pH values. Mikrochim. Acta 185 (1), 57.

Fu, S., Zhu, C., Song, J., Engelhard, M., Xia, H., Du, D., Lin, Y., 2016. PdCuPt nanocrystals with multibranches for enzyme-free glucose detection. ACS Appl. Mater. Interfaces 8 (34), 22196–22200.

Gao, J., Huang, W., Chen, Z., Yi, C., Jiang, L., 2019. Simultaneous detection of glucose, uric acid and cholesterol using flexible microneedle electrode array-based biosensor and multi-channel portable electrochemical analyzer. Sens. Actuators, B 287, 102–110.

Guo, Z., Seol, M.L., Kim, M.S., Ahn, J.H., Choi, Y.K., Liu, J.H., Huang, X.J., 2012. Hollow CuO nanospheres uniformly anchored on porous Si nanowires: preparation and their potential use as electrochemical sensors. Nanoscale 4 (23), 7525–7531.

Han, T., Zhu, S., Wang, S., Wang, B., Zhang, X., Wang, G., 2019. Fluorometric methods for determination of H_2O_2, glucose and cholesterol by using MnO_2 nanosheets modified with 5-carboxyfluorescein. Mikrochim. Acta 186 (5), 269.

He, L., Jiang, Z.W., Li, W., Li, C.M., Huang, C.Z., Li, Y.F., 2018. In situ synthesis of gold nanoparticles/metal-organic gels hybrids with excellent peroxidase-like activity for sensitive chemiluminescence detection of organophosphorus pesticides. ACS Appl. Mater. Interfaces 10 (34), 28868–28876.

He, L., Peng, Z.W., Jiang, Z.W., Tang, X.Q., Huang, C.Z., Li, Y.F., 2017. Novel iron(III)-Based Metal−Organic gels with superior catalytic performance toward luminol chemiluminescence. ACS Appl. Mater. Interfaces 9 (37), 31834–31840.

Hu, L., Huang, Y., Zhang, F., Chen, Q., 2013. CuO/Cu_2O composite hollow polyhedrons fabricated from metal-organic framework templates for lithium-ion battery anodes with A long cycling life. Nanoscale 5 (10), 4186–4190.

Hu, X.S., Li, C., Lou, X.B., Yang, Q., Hu, B.W., 2017a. Hierarchical CuO octahedra inherited from copper metal-organic frameworks: high-rate and high-capacity lithium-ion storage materials stimulated by pseudocapacitance. J. Mater. Chem. A. 5 (25), 12828–12837.

Hu, Y., Cheng, H., Zhao, X., Wu, J., Muhammad, F., Lin, S., He, J., Zhou, L., Zhang, C., Deng, Y., Wang, P., Zhou, Z., Nie, S., Wei, H., 2017b. Surface-enhanced Raman scattering active gold nanoparticles with enzyme-mimicking activities for measuring glucose and lactate in living tissues. ACS Nano 11 (6), 5558–5566.

Huang, J., Zhu, Y., Zhong, H., Yang, X., Li, C., 2014. Dispersed CuO nanoparticles on A silicon nanowire for improved performance of nonenzymatic H_2O_2 detection. ACS Appl. Mater. Interfaces 6 (10), 7055–7062.

Huang, J.F., Li, H., Zhu, Y.H., Cheng, Q.L., Yang, X.L., Li, C.Z., 2015. Sculpturing metal foams toward bifunctional 3D copper oxide nanowire arrays for pseudo-capacitance and enzyme-free hydrogen peroxide detection. J. Mater. Chem. 3 (16), 8734–8741.

Huang, Y., Zhao, M., Han, S., Lai, Z., Yang, J., Tan, C., Ma, Q., Lu, Q., Chen, J., Zhang, X., Zhang, Z., Li, B., Chen, B., Zong, Y., Zhang, H., 2017. Growth of Au nanoparticles on 2D metalloporphyrinic metal-organic framework nanosheets used as biomimetic catalysts for cascade reactions. Adv. Mater. 29 (32), 1700102.

Jana, S., Mondal, A., Ghosh, A., 2018. Fabrication of stable NiO/Fe_2O_3 heterostructure: a versatile hybrid material for electrochemical sensing of glucose, methanol and enhanced photodecomposition and/photoreduction of water contaminants. Appl. Catal. B Environ. 232, 26–36.

Jayaramulu, K., Geyer, F., Petr, M., Zboril, R., Vollmer, D., Fischer, R.A., 2017. Shape controlled hierarchical porous hydrophobic/oleophilic metal-organic nanofibrous gel composites for oil adsorption. Adv. Mater. 29 (12), 1605307.

Kamtekar, K.T., Monkman, A.P., Bryce, M.R., 2010. Recent advances in white organic light-emitting materials and devices (WOLEDs). Adv. Mater. 22 (5), 572–582.

Karan, C.K., Bhattacharjee, M., 2016. Self-healing and moldable metallogels as the recyclable materials for selective dye adsorption and separation. ACS Appl. Mater. Interfaces 8 (8), 5526–5535.

Ko, S., Lee, J.I., Yang, H.S., Park, S., Jeong, U., 2012. Mesoporous CuO particles threaded with CNTs for high-performance lithium-ion battery anodes. Adv. Mater. 24 (32), 4451–4456.

Komathi, S., Muthuchamy, N., Lee, K.P., Gopalan, A.I., 2016. Fabrication of A Novel dual mode cholesterol biosensor using titanium dioxide nanowire bridged 3D graphene nanostacks. Biosens. Bioelectron. 84, 64–71.

Li, X.M., Li, J.Y., Gao, Y., Kuang, Y., Shi, J.F., Xu, B., 2010. Molecular nanofibers of olsalazine form supramolecular hydrogels for reductive release of an anti-inflammatory agent. J. Am. Chem. Soc. 132, 17707–17709.

Li, Y., Jiang, Z.W., Xiao, S.Y., Huang, C.Z., Li, Y.F., 2018. Terbium(III) organic gels: novel antenna effect-induced enhanced electrochemiluminescence emitters. Anal. Chem. 90 (20), 12191–12197.

Liang, H., Xiao, K., Wei, L., Yang, B., Yu, G., Deng, S., Duan, H., Zhu, C., Li, J., Zhang, J., 2019. Decomplexation removal of Ni(II)-Citrate complexes through heterogeneous fenton-like process using novel CuO-CeO_2-CoO_x composite nanocatalyst. J. Hazard Mater. 374, 167–176.

Lin, K.L., Yang, T., Zhang, F.F., Lei, G., Zou, H.Y., Li, Y.F., Huang, C.Z., 2017. Luminol and gold nanoparticle-Co-precipitated reduced graphene oxide hybrids with long-persistent chemiluminescence for cholesterol detection. J. Mater. Chem. B 5 (35), 7335–7341.

Lin, Q., Lu, T.T., Zhu, X., Wei, T.B., Li, H., Zhang, Y.M., 2016. Rationally introduce multi-competitive binding interactions in supramolecular gels: a simple and efficient approach to develop multi-analyte sensor array. Chem. Sci. 7 (8), 5341–5346.

Lin, T.R., Qin, Y.M., Huang, Y.L., Yang, R.T., Hou, L., Ye, F.G., Zhao, S.L., 2018. A label-free fluorescence assay for hydrogen peroxide and glucose based on the bifunctional MIL-53(Fe) nanozyme. Chem. Commun. 54 (14), 1762–1765.

Ling, P.H., Zhang, Q., Cao, T.T., Gao, F., 2018. Versatile three-dimensional porous Cu@Cu_2O aerogel networks as electrocatalysts and mimicking peroxidases. Angew. Chem. Int. Ed. 57 (23), 6819–6824.

Liu, X., Wang, Q., Zhao, H.H., Zhang, L.C., Su, Y.Y., Lv, Y., 2012. BSA-templated MnO_2 nanoparticles as both peroxidase and oxidase mimics. Analyst 137 (19), 4552.

Martin, L., Martinez, H., Poinot, D., Pecquenard, B., Cras, F.L., 2013. Comprehensive X-ray photoelectron spectroscopy study of the conversion reaction mechanism of CuO in lithiated thin film electrodes. J. Phys. Chem. C 117 (9), 4421–4430.

Meng, F., Shi, W., Sun, Y., Zhu, X., Wu, G., Ruan, C., Liu, X., Ge, D., 2013. Nonenzymatic biosensor based on Cu_xO nanoparticles seposited on polypyrrole nanowires for improving detection range. Biosens. Bioelectron. 42, 141–147.

Muench, F., Sun, L., Kottakkat, T., Antoni, M., Schaefer, S., Kunz, U., Molina-Luna, L., Duerrschnabel, M., Kleebe, H.J., Ayata, S., Roth, C., Ensinger, W., 2017. Free-standing networks of core-shell metal and metal oxide nanotubes for glucose sensing. ACS Appl. Mater. Interfaces 9 (1), 771–781.

Natalio, F., Andre, R., Hartog, A.F., Stoll, B., Jochum, K.P., Wever, R., Tremel, W., 2012. Vanadium pentoxide nanoparticles mimic vanadium haloperoxidases and thwart biofilm formation. Nat. Nanotechnol. 7 (8), 530–535.

Peng, Y., L.D., Q., J.G., J., X.Y., H., D.L., M., 2018. Flexible fiber-shaped non-enzymatic sensors with A graphene-metal heterostructure based on graphene fibres decorated with gold nanosheets. Carbon 136, 329–336.

Poizot, P., Laruelle, S., Grugeon, S., Dupont, L., Tarascon, J.M., 2000. Nano-sized transition-metal oxides as negative-electrode materials for lithium-ion batteries. Nature 407 (5), 496–499.

Reddy, K.R., Brahman, P.K., Suresh, L., 2018. Fabrication of high performance disposable screen printed electrochemical sensor for ciprofloxacin sensing in biological samples. Measurement 127, 175–186.

Sedighi, A., Montazer, M., Mazinani, S., 2019. Synthesis of wearable and flexible NiP0.1-SnO_x/PANI/CuO/cotton towards A non-enzymatic glucose sensor. Biosens. Bioelectron. 135, 192–199.

Shih, Y.H., Chen, J.H., Lin, Y., Chen, H.T., Lin, C.H., Huang, H.Y., 2017. Nitrogen-doped porous carbon material derived from metal-organic gel for small biomolecular sensing. Chem. Commun. 53 (42), 5725–5728.

Shrestha, B.K., Ahmad, R., Shrestha, S., Park, C.H., Kim, C.S., 2017. In situ synthesis of cylindrical spongy polypyrrole doped protonated graphitic carbon nitride for cholesterol sensing application. Biosens. Bioelectron. 94, 686–693.

Shu, Y., Li, B., Chen, J., Xu, Q., Pang, H., Hu, X., 2018. Facile synthesis of ultrathin nickel-cobalt phosphate 2D nanosheets with enhanced electrocatalytic activity for glucose oxidation. ACS Appl. Mater. Interfaces 10 (3), 2360–2367.

Song, C., Zhao, Z., Sun, X., Zhou, Y., Wang, Y., Wang, D., 2019. In Situ Growth of Ag Nanodots Decorated Cu2O Porous Nanobelts Networks on Copper Foam for Efficient HER Electrocatalysis. Small 15 (29) 1804268.

Sun, Y., Giebink, N.C., Kanno, H., Ma, B., Thompson, M.E., Forrest, S.R., 2006.

Management of singlet and triplet excitons for efficient white organic light-emitting devices. Nature 440 ( ) (7086), 908–912.
Suresh, L., Brahman, P.K., Reddy, K.R., J, S.B., 2018. Development of an electrochemical immunosensor based on gold nanoparticles incorporated chitosan biopolymer nanocomposite film for the detection of prostate cancer using PSA as biomarker. Enzym. Microb. Technol. 112, 43–51.
Tam, A.Y., Yam, V.W., 2013. Recent advances in metallogels. Chem. Soc. Rev. 42 (4), 1540–1567.
Tan, S.Y., Ang, C.Y., Mahmood, A., Qu, Q.Y., Li, P.Z., Zou, R.Q., Zhao, Y.L., 2016. Doxorubicin-loaded metal–organic gels for pH and glutathione dual-responsive release. ChemNanoMat 2 (6), 504–508.
Tanaka, S., Kaneti, Y.V., Bhattacharjee, R., Islam, M.N., Nakahata, R., Abdullah, N., Yusa, S.I., Nguyen, N.T., Shiddiky, M.J.A., Yamauchi, Y., Hossain, M.S.A., 2018. Mesoporous iron oxide synthesized using poly(styrene-b-acrylic acid-b-ethylene glycol) block copolymer micelles as templates for colorimetric and electrochemical detection of glucose. ACS Appl. Mater. Interfaces 10 (1), 1039–1049.
Wang, L., Ke, F., Zhu, J., 2016. Metal-organic gel templated synthesis of magnetic porous carbon for highly efficient removal of organic dyes. Dalton Trans. 45 (11), 4541–4547.
Wang, Z., Su, F., Madhavi, S., Lou, X.W., 2011. CuO nanostructures supported on Cu substrate as integrated electrodes for highly reversible lithium storage. Nanoscale 3 (4), 1618–1623.
Wang, Z., Yan, T.T., Chen, G.R., Shi, L.Y., Zhang, D.S., 2017. High salt removal capacity of metal–organic gel derived porous carbon for capacitive deionization. ACS Sustain. Chem. Eng. 5 (12), 11637–11644.
Wang, Z.H., Jin, H.H., Meng, T., Liao, K., Meng, W.Q., Yang, J.L., He, D.P., Xiong, Y.L., Mu, S.C., 2018. Fe, Cu-coordinated ZIF-derived carbon framework for efficient oxygen reduction reaction and zinc-air batteries. Adv. Funct. Mater. 28 (39), 1802596.
Wu, H., Zheng, J., Kjoniksen, A.L., Wang, W., Zhang, Y., Ma, J., 2019a. Metallogels: availability, applicability, and advanceability. Adv. Mater. 31 (12), 1806204.
Wu, H.X., Cao, W.M., Li, Y., Liu, G., Wen, Y., Yang, H.F., Yang, S.P., 2010. In situ growth of copper nanoparticles on multiwalled carbon nanotubes and their application as non-enzymatic glucose sensor materials. Electrochim. Acta 55 (11), 3734–3740.
Wu, J.J.X., Wang, X.Y., Wang, Q., Lou, Z.P., Li, S.R., Zhu, Y.Y., Qin, L., Wei, H., 2019b. Nanomaterials with enzyme-like characteristics (nanozymes): next-generation artificial enzymes (II). Chem. Soc. Rev. 48 (4), 1004–1076.
Xiao, S., Pan, D., Wang, L., Zhang, Z., Lyu, Z., Dong, W., Chen, X., Zhang, D., Chen, W., Li, H., 2016. Porous CuO nanotubes/graphene with sandwich architecture as high-performance anodes for lithium-ion batteries. Nanoscale 8 (46), 19343–19351.
Xu, J., Li, F., Wang, D., Nawaz, M.H., An, Q., Han, D., Niu, L., 2019. Co_3O_4 nanostructures on flexible carbon cloth for crystal plane effect of nonenzymatic electrocatalysis for glucose. Biosens. Bioelectron. 123, 25–29.
Yang, D.H., Kong, L., Zhong, M., Zhu, J., Bu, X.H., 2018. Metal-organic gel-derived Fe_xO_y/nitrogen-doped carbon films for enhanced lithium storage. Small 15 (3), 1804058.
Yang, J., Ye, H., Zhao, F., Zeng, B., 2016. A novel CuxO Nanoparticles@ZIF-8 composite derived from core-shell metal-organic frameworks for highly selective electrochemical sensing of hydrogen peroxide. ACS Appl. Mater. Interfaces 8 (31), 20407–20414.
Yao, J., Cheng, Y., Zhou, M., Zhao, S., Lin, S., Wang, X., Wu, J., Li, S., Wei, H., 2018. ROS scavenging Mn_3O_4 nanozymes for in vivo anti-inflammation. Chem. Sci. 9 (11), 2927–2933.
Yin, W., Ma, D., Yu, J., Zhang, X., Mei, L., Zu, Y., An, L., Gu, Z., 2018. Synthesis of surface modification oriented nano-sized molybdenum disulfide with high peroxidase-like catalytic activity for H_2O_2 and cholesterol detection. Chem. Eur J. 24 (59), 15868–15878.
Yuan, Z.Q., Wang, Y., Qian, Y.T., 2012. A facile room-temperature route to flower-like CuO microspheres with greatly enhanced lithium storage capability. RSC Adv. 2 (23), 8602–8605.
Zeng, Q.X., Xu, G.C., Zhang, L., Lin, H., Lv, Y., Jia, D.Z., 2018. Porous CuO nanofibers derived from A Cu-based coordination polymer as A photocatalyst for the degradation of rhodamine B. New J. Chem. 42 (9), 7016–7024.
Zhang, X., Qin, W., Li, D., Yan, D., Hu, B., Sun, Z., Pan, L., 2015. Metal-organic framework derived porous CuO/Cu_2O composite hollow octahedrons as high performance anode materials for sodium ion batteries. Chem. Commun. 51 (91), 16413–16416.
Zhang, Y., Wang, Y.N., Sun, X.T., Chen, L., Xu, Z.R., 2017. Boron nitride nanosheet/CuS nanocomposites as mimetic peroxidase for sensitive colorimetric detection of cholesterol. Sens. Actuators, B 246, 118–126.
Zheng, J.Z., Zhang, W.X., Lin, Z.Q., Wei, C., Yang, W.Z., Dong, P.H., Yan, Y.R., Hu, S.R., 2016. Microwave synthesis of 3D rambutan-like CuO and CuO/reduced graphene oxide modified electrodes for non-enzymatic glucose detection. J. Mater. Chem. B 4 (7), 1247–1253.
Zheng, S., Li, B., Tang, Y., Li, Q., Xue, H., Pang, H., 2018. Ultrathin nanosheet-assembled $[Ni_3(OH)_2(PTA)_2(H_2O)_4].2H_2O$ hierarchical flowers for high-performance electrocatalysis of glucose oxidation reactions. Nanoscale 10 (27), 13270–13276.
Zhuang, Y., Zhang, X., Chen, Q., Li, S., Cao, H., Huang, Y., 2019. Co_3O_4/CuO hollow nanocage hybrids with high oxidase-like activity for biosensing of dopamine. Mater. Sci. Eng. C 94, 858–866.